

# Swept-Source Anatomic Optical Coherence Elastography of Porcine Trachea

Ruofei Bu<sup>a</sup>, Hillel Price<sup>b</sup>, Sorin Mitran<sup>c</sup>, Carlton Zdanski<sup>d</sup>, Amy L. Oldenburg<sup>a,b,e</sup>  
<sup>a</sup> Department of Biomedical Engineering; <sup>b</sup> Department of Physics and Astronomy; <sup>c</sup> Department of Mathematics; <sup>d</sup> Department of Otolaryngology/Head and Neck Surgery; <sup>e</sup> Biomedical Research Imaging Center;  
University of North Carolina at Chapel Hill, North Carolina, USA, 27599

Conference: SPIE Photonics West BIOS 2016 (BO102 Optical Imaging, Therapeutics, and Advanced Technology in Head and Neck Surgery and Otolaryngology)

## ABSTRACT

Quantitative endoscopic imaging is at the vanguard of novel techniques in the assessment upper airway obstruction. Anatomic optical coherence tomography (aOCT) has the potential to provide the geometry of the airway lumen with high-resolution and in 4 dimensions. By coupling aOCT with measurements of pressure, optical coherence elastography (OCE) can be performed to characterize airway wall stiffness. This can aid in identifying regions of dynamic collapse as well as informing computational fluid dynamics modeling to aid in surgical decision-making.

Toward this end, here we report on an anatomic optical coherence tomography (aOCT) system powered by a wavelength-swept laser source. The system employs a fiber-optic catheter with outer diameter of 0.82 mm deployed via the bore of a commercial, flexible bronchoscope. Helical scans are performed to measure the airway geometry and to quantify the cross-sectional-area (CSA) of the airway. We report on a preliminary validation of aOCT for elastography, in which aOCT-derived CSA was obtained as a function of pressure to estimate airway wall compliance. Experiments performed on a Latex rubber tube resulted in a compliance measurement of  $0.68 \pm 0.02 \text{ mm}^2/\text{cmH}_2\text{O}$ , with  $R^2=0.98$  over the pressure range from 10 to 40 cmH<sub>2</sub>O. Next, ex vivo porcine trachea was studied, resulting in a measured compliance from  $1.06 \pm 0.12$  to  $3.34 \pm 0.44 \text{ mm}^2/\text{cmH}_2\text{O}$ , ( $R^2 > 0.81$ ). The linearity of the data confirms the elastic nature of the airway. The compliance values are within the same order-of-magnitude as previous measurements of human upper airways, suggesting that this system is capable of assessing airway wall compliance in future human studies.

**Keywords:** anatomic optical coherence tomography, elastography, airway wall compliance

## 1. INTRODUCTION

Upper airway obstructive disorder (UAOD) is a common problem associated with considerable health risks. Upper airway obstruction commonly studied that affect children include subglottic stenosis (SGS) and Pierre Robin Sequence (PRS), while obstructive sleep apnea (OSA)<sup>1,2,3</sup> is widely prevalent amongst the adult population. Compared with adults, infants and young children have small and compliant airways and can quickly develop clinically significant upper airway obstruction<sup>4</sup>. At the moment, the gold standard procedure for evaluation of the airway is endoscopy. With the help of an endoscope, abnormalities like narrowing or obstruction of the airways are identified to aid in diagnosis and treatment planning. However, endoscopy only provides qualitative and semi-quantitative data at best. In comparison, computed tomography (CT) and magnetic resonance imaging (MRI) permit quantification of the airway luminal geometry, but CT produces ionizing radiation, and MRI require sedation for pediatric patients, which poses risk particularly for children with UAOD<sup>5,6</sup>. Furthermore, 4 dimensional imaging of airway deformation during breathing, including dynamic collapse events, is highly limited due to relatively poor spatial and temporal resolution, particularly with MRI.

Optical coherence tomography (OCT) is well-suited to address these shortcomings. OCT is a near-infrared light imaging technique based on low-coherence interferometry, which achieves precise axial sectioning in highly scattering

Photonic Therapeutics and Diagnostics XII, edited by Bernard Choi, et al., Proc. of SPIE  
Vol. 9689, 968923 · © 2016 SPIE · CCC code: 1605-7422/16/\$18 · doi: 10.1117/12.2213186

media<sup>7</sup>. OCT resolves structures at micrometer-level resolution<sup>8</sup> while offering high imaging speed and no health risks. While OCT is a relatively mature microscopic imaging technology in other application areas, it has not yet been fully adapted to the need for long-range imaging (>2 mm and up to 30 mm) needed for anatomic airway imaging. For this reason, “anatomic” OCT was originally developed using time-domain OCT technology for quantitative upper airway imaging<sup>9</sup>. More recently, swept-source aOCT systems have been employed to provide 4 dimensional upper airway imaging<sup>10</sup>. Studies in the past few decades using aOCT for human airway imaging include those of the *in vivo* human larynx<sup>11</sup>, upper respiratory tract<sup>12,13</sup>, lower airways<sup>14</sup>, pulmonary imaging and diagnosis<sup>15</sup> and abnormal bronchial lesions<sup>16</sup>. For structural characteristics of the airway lumen, aOCT has been performed for upper respiratory tract imaging<sup>12</sup>, pharyngeal shape and size evaluation<sup>9</sup> and airway dimension measurements<sup>17</sup>. Also aOCT allows study over lengthy periods during both sleep and wakefulness<sup>18</sup>, which makes it the ideal tool for diagnosing and studying UAOD.

Quantifying the mechanical properties of the upper airway can aid in better understanding the mechanisms of dynamic collapse in UAOD. For example, regions of highly compliant airway wall tissue have been associated with collapse in obstructive sleep apnea (OSA)<sup>19</sup>. Studies have shown that the most compliant part of the upper airway in the majority of individuals is the velopharynx, and the shape and size change with pressure drop across the pharynx can be used to evaluate the capacity of flow characteristics to identify individuals with and without OSA<sup>20</sup>. Thus, measuring tissue compliance is extremely important in understanding this dynamic behavior. Compliance is commonly measured in respiratory physiology, which is related to airflow resistance and gas exchange<sup>21</sup>, and is defined as the change in volume divided by the change in pressure<sup>22</sup>. In clinical practice, cross-sectional compliance (CC) is utilized, which assumes that there is no significant change to the length of the airway under applied pressure, and therefore volume changes are proportional to changes in CSA<sup>23</sup>. In this paper we will use also this convention, exclusively reporting cross-sectional compliance.

Here we report the use of a portable aOCT system which can be delivered via commercially available bronchoscopes for upper airway structural imaging, and investigate its potential to extract elastic airway properties. The measurement of deformation under applied pressure allows one to generate an elastography map<sup>24</sup>. Elastography using anatomic OCT has previously been performed in central airways<sup>19</sup>, and measurements of airway wall deformation versus pressure have been performed in the upper airways of people suffering from sleep apnea<sup>20</sup>. As aOCT provides higher resolution compared with CT and MRI, it is expected that aOCT would yield more accurate measurements of deformation, and consequently compliance, using aOCT. In this paper, we measure axial CSA-based compliance changes at different positions on the sagittal plane, slice-by-slice. However, we recognize that compliance also varies within each slice plane, and future methods will be developed to assess this type of inter-slice heterogeneity. A primary strength of performing elastography using aOCT is the possibility to integrate it into a standard clinical bronchoscope. Coupling aOCT with bronchoscopy, (which is a mature, safe, and widely used diagnostic modality) could be very useful for scientifically and clinically studying upper airway biomechanical properties and possibly aid in medical and surgical decision-making.

This manuscript focuses on two aspects of aOCT development coupled with endoscopy for evaluation of the airway: 1) validation of geometry obtained by aOCT in static samples; and 2) exploration of compliance measurements as a first step towards full elastography of the airway. For these studies we employed phantoms and *ex vivo* porcine tracheas to test the aOCT system, and compared the results with either other measurements or theoretical values to verify the accuracy of the system.

## 2. METHODS

### 2.1 Swept Source aOCT system

The anatomic optical coherence (aOCT) system is powered by a swept laser source (HSL-2100-LC Santec Inc.) operating at 5 kHz with a 1310 nm center wavelength and 30 nm sweep range. The output power of the infrared laser beam is 16.5mW, and the coherence length is 17.5mm. The beam is directed via single-mode fiber into a Mach-Zehnder interferometer, and a balanced photo-detector with 75MHz bandwidth is used for detecting back-scattered signals from the sample and reference arms. The fiber-optic scanner is equipped with a stepper motor for translational motion and a DC motor for rotation to control the helical pull-back of the catheter in the sample arm. The catheter is introduced into the side port of a standard flexible bronchoscope (STORZ 11003BC).

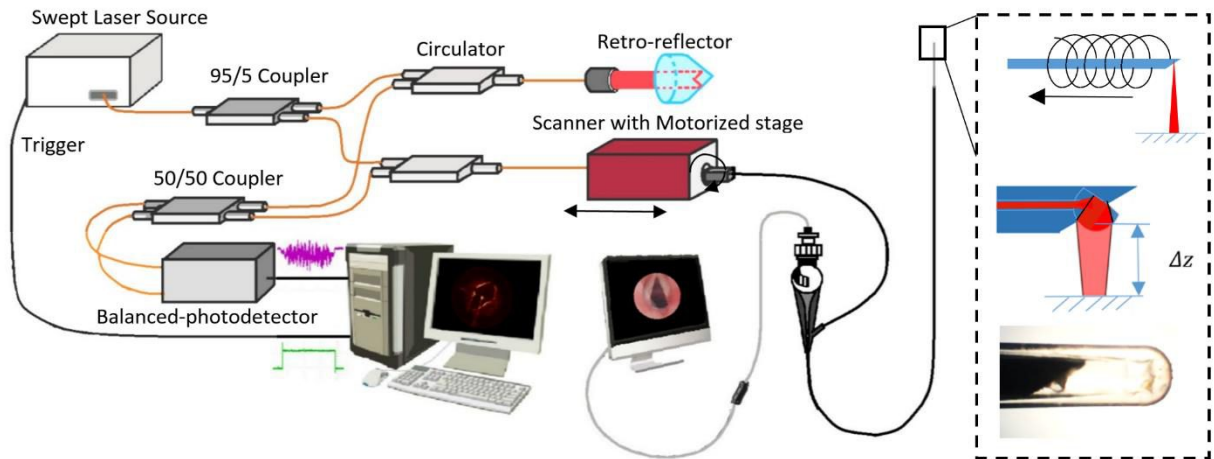


Figure 1. Anatomic OCT system hardware diagram

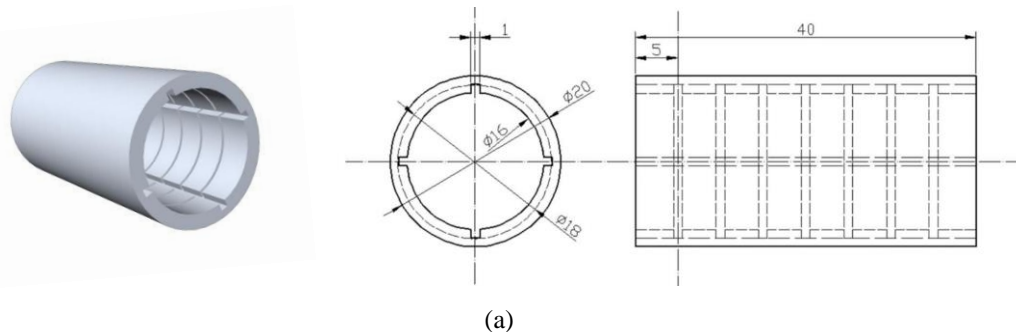
The axial resolution of the system is  $25.6\mu\text{m}$ , and the transverse resolution ranges from  $100\text{-}400\mu\text{m}$  over the axial distance from  $2.7\text{ mm}$  to  $12\text{ mm}$ . The signal to noise ratio (SNR) of the system exhibits a roll-off with imaging depth, starting at  $98\text{ dB}$  at  $2\text{ mm}$  and decreasing to  $81\text{ dB}$  within at  $11\text{ mm}$ . The pull-back speed of the catheter was set to  $3\text{ mm/s}$ , and the rotational speed was set to  $10\text{ Hz}$ , corresponding to a  $0.3\text{ mm}$  distance between each slice. The fiber-optic catheter (Physical Sciences, Inc) is  $170\text{ cm}$  long with an outer diameter (including the protective tube) of  $0.82\text{ mm}$ , and contains a ball-lens structure at the distal tip (Fig.1). To protect the catheter from airway surface fluid, a plastic sheath with an epoxy-sealed tip is used, which easily fits into the working channel of the bronchoscope.

A digitizer (ATS 9440, AlazarTech Inc.) with a  $10\text{ Ms/s}$  real-time sampling rate is used for data acquisition, and a program written in LabVIEW controls the scanner engine and data acquisition. The swept laser source features high scan linearity with high repeatability, which means no k-clock sampling is needed, and only an algorithm-based dispersion compensation solution is applied to improve the system performance<sup>25</sup>. In OCE experiments, a bag-valve mask (BVM) is used to provide air pressure to quantify airway mechanical properties.

### 3. ANATOMICAL IMAGING

#### 3.1 aOCT and CT of a Tube phantom

To verify the accuracy of the system, a plastic tube with internal ring structures and four  $90^\circ$  notches was used as the subject, and aOCT and CT images were collected. The aOCT pull-back distance was  $\sim 25\text{ mm}$ , and corresponding 3D reconstructions of the inner surface were obtained for both aOCT and CT (Fig. 2). The results qualitatively show that aOCT provides higher resolution compared with CT scan, as the aOCT reconstruction exhibits most of the detailed ring structures and some of the notches, while these structures are difficult to detect from the CT reconstruction. Also, the pixel sizes are much larger for the CT reconstruction ( $0.447\text{ mm}$ ) compared to that of the aOCT reconstruction ( $0.05\text{ mm}$ ), leading to an uneven and staircase appearance for the CT reconstruction.



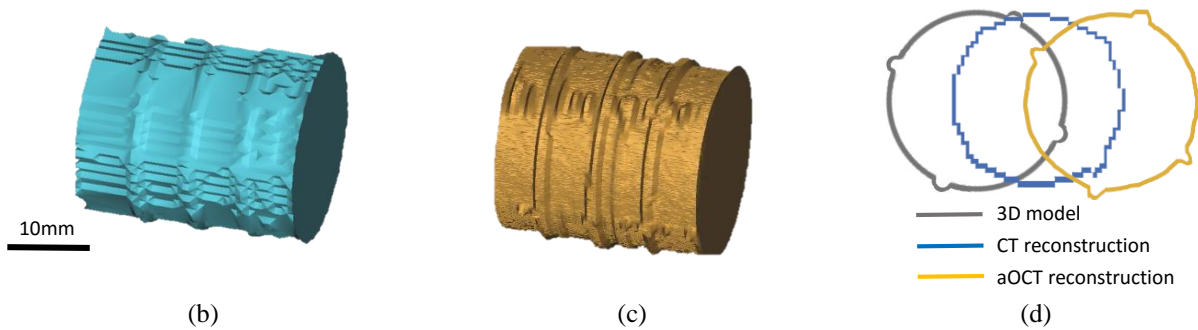
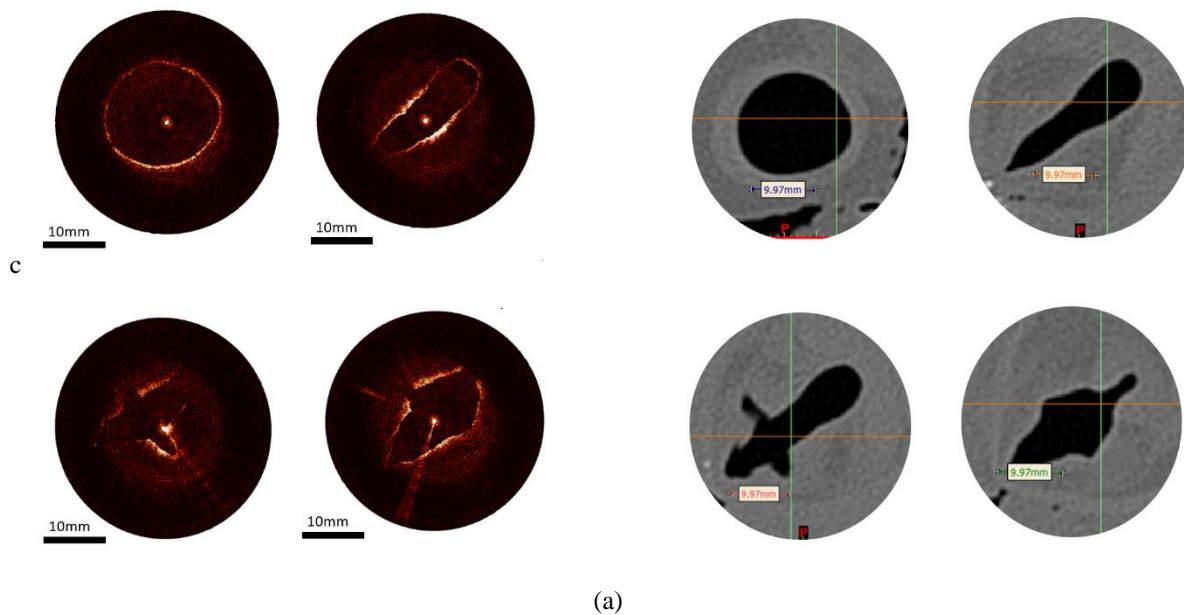


Figure 2. a) 3D model of the plastic tube; b) 3D reconstruction from CT scan; c) 3D reconstruction from aOCT scan; d) CSA of the original model, CT scan and aOCT scan

### 3.2 aOCT and CT of *ex vivo* porcine trachea

Although the tests in the previous section are promising, it is recognized that the optical properties of tissues are quite different from those of plastic. Due to the irregular shape of the trachea, a CT scan is used to verify the accuracy of the aOCT scan. An *ex vivo* experiment was performed using porcine trachea. We chose imaging positions with characteristic structures including the true and false vocal folds, the laryngeal ventricles, and the subglottis. Based on the qualitative comparison between the two imaging techniques, the main structures appear to be well-represented with aOCT, which indicates it is capable of providing upper airway geometry.



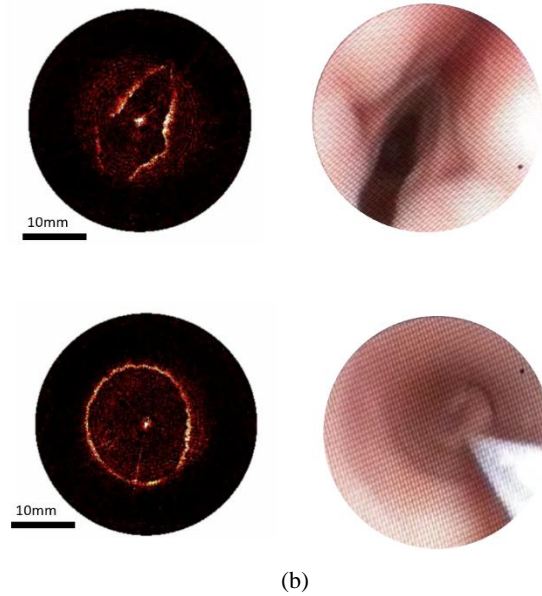


Figure 3. a) Porcine trachea images from aOCT and CT; b) Porcine trachea images from aOCT and endoscopy display screen.

## 4. ELASTOGRAPHY

Elastography is a process of estimating elastic properties of tissues through imaging techniques<sup>26</sup>. Here we perform a validation experiment to assess the ability of the aOCT system to measure a single value of compliance at each cross-sectional area (using the CC definition of compliance); in future work we plan to extend this to true “elastography” mapping of wall compliance at individual positions on the airway wall. We started by examining the compliance of tube phantoms with known properties to test the system’s ability to measure compliance, and then used the system on freshly excised porcine trachea. As the modulus of elasticity varies with the amount of load, the direction in which the load is applied, and heterogeneous structures like tracheal cartilage rings<sup>27</sup>, there are no readily available methods to cross-validate our OCE methods in tissues. Instead, we provide semi-quantitative comparisons with known tracheal measurements in this study.

### 4.1 Compliance of a tube phantom

To test the precision of the system for measuring compliance, we first employed a phantom with known mechanical properties. To simulate the compliance of the human upper airway, we chose Latex rubber as the material as it is highly compliant. The shape of the phantom is a thin-walled cylindrical tube of similar diameter to that of a trachea. Based on elasticity theory, the compliance can be calculated using a thin-wall model<sup>28</sup>.

The axial, circumferential and radial components of the stress tensor ( $\sigma_a$ ,  $\sigma_c$  and  $\sigma_r$  respectively) applied on the wall can be calculated by the formulas:

$$\sigma_a = \frac{p_i a^2 - p_o b^2}{b^2 - a^2}$$

$$\sigma_c = -\frac{a^2 b^2 (p_o - p_i)}{b^2 - a^2} \cdot \frac{1}{r^2} + \frac{p_i a^2 - p_o b^2}{b^2 - a^2}$$

$$\sigma_r = \frac{a^2 b^2 (p_o - p_i)}{b^2 - a^2} \cdot \frac{1}{r^2} + \frac{p_i a^2 - p_o b^2}{b^2 - a^2}$$

In the above:  $a$  is the inner diameter;  $b$  is the outer diameter;  $p_i$  is the inner pressure; and  $p_o$  is the outer pressure. The radial strain is then defined as:  $\epsilon_r = \frac{\sigma_r - \nu(\sigma_a + \sigma_c)}{E}$ , where  $E$  is the Young’s modulus of the material, and  $\nu$  is Poisson’s ratio.

Using the CC definition of compliance:

$$C = \frac{\Delta CSA}{\Delta dp} \Big|_{dp=0} = \frac{2a^2\pi[b^2(v+1) + a^2(-1+2v)]}{(a^2 - b^2)E}$$

where the change of pressure is  $dp = p_o - p_i$ . By using this model, and the estimated Young's modulus of the Latex rubber as 600 kPa, we estimated the theoretical compliance of the tube phantom to be 0.78 mm<sup>2</sup>/cmH<sub>2</sub>O.

We then performed aOCT to determine the experimental compliance value. We pressurized the tube to values of 0, 20, 30, 40 and 60 cmH<sub>2</sub>O, and collected CSA data under each pressure. As there was no pre-compression at 0 pressure, and pressure leakage in the system at 60 cmH<sub>2</sub>O pressure, we excluded those measurements from the linear fitting. The slope of the best-fit line (left panel of Fig. 4) was used for each pressure curve to determine the CC compliance. aOCT scans were performed at five different positions along the tube (from 0mm to 48mm). As gaps between slices were very small (0.3mm) compared with the distance between each scan (12mm), three adjacent slices within each scan were used to independently measure the compliance, from which the mean and standard deviation of the compliance was computed (Fig. 4, right panel). The standard deviation value at each position represents the precision of our experiment, and is related to random error in the system at a given position. As shown in Table 1, the standard deviations are all less than ±0.027 mm<sup>2</sup>/cmH<sub>2</sub>O, corresponding to 4.1%. Across the length of the tube, the mean value of compliance was 0.68 mm<sup>2</sup>/cmH<sub>2</sub>O with overall standard deviation of 0.022 mm<sup>2</sup>/cmH<sub>2</sub>O, corresponding to a difference along the length of the tube of less than 5.4%; part of this error may arise from heterogeneity in the tube itself. Also, Table 1 shows the average R<sup>2</sup> value obtained for each set of CC data. The high linearity (R<sup>2</sup>> 0.98) of the CSA-pressure data is consistent with the elastic nature of the Latex rubber. Finally, the mean compliance value is reasonably consistent with the theoretical value of the phantom (within 15%), given uncertainty in the exact Young's modulus of the Latex material. Further study using a tube of well-known Young's modulus is needed to further validate the accuracy of compliance measurement with the aOCT system.

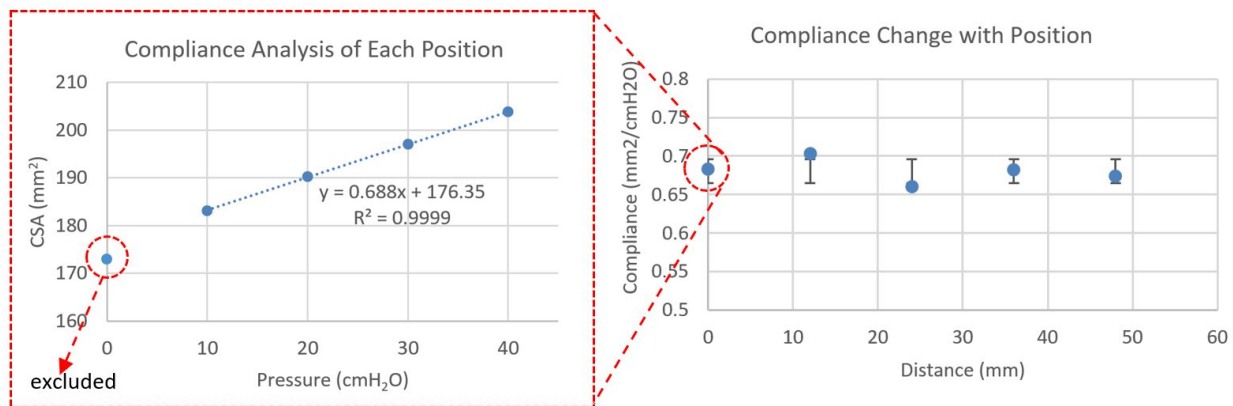


Figure 4. Tube phantom compliance results. The left panel shows an example calculation of the compliance from the slope of the fitted line in pneumatic units. The right graph summarizes the compliance measured at each position.

Table 1. Compliance value for Latex Rubber tube at five different positions

| Position (mm)                                    | 0           | 12          | 24          | 36          | 48          |
|--|-------------|-------------|-------------|-------------|-------------|
| Compliance (mm <sup>2</sup> /cmH <sub>2</sub> O) | 0.683±0.008 | 0.703±0.014 | 0.660±0.027 | 0.682±0.025 | 0.674±0.024 |
| R <sup>2</sup>                                   | 0.998       | 0.995       | 0.983       | 0.985       | 0.988       |

#### 4.2 Compliance of an *ex vivo* trachea

We performed an *ex vivo* experiment to further test the ability to measure upper airway compliance with aOCT. An elongated upper airway was prepared by suturing together 3 smaller pieces of fresh porcine trachea. No gas leakage was found after the suturing. We measured compliance at 6 different positions (as shown in Fig 5), among which we successfully obtained three sets of data which had sufficiently stable pressure for further analysis. Fig 6 shows the CSA changes at three positions under different pressure values, which illustrate the pressure-dependent expansion of the airway wall.

Based on the results displayed in Table 3, the linear regression analysis of the compliance data exhibits high linearity, with  $R^2 > 0.81$  across all measurements. This confirms the elastic nature of the airway under these quasi-static deformations. The measured compliance value varied at different positions (as shown in Fig 7) from 1.06 to 3.34mm<sup>2</sup>/cmH<sub>2</sub>O, which may be due to heterogeneity in the airway wall properties. These compliance values are slightly smaller than that from previous measurements of human upper airway, which range from 4.1 to 9.7mm<sup>2</sup>/cmH<sub>2</sub>O for normal/healthy airways and 2.2 to 12.3 for patients with OSA<sup>18</sup>. Since our measured compliance values are within the same order-of-magnitude as that of human upper airways, we expect that this system will be capable of assessing airway wall compliance in future human studies.

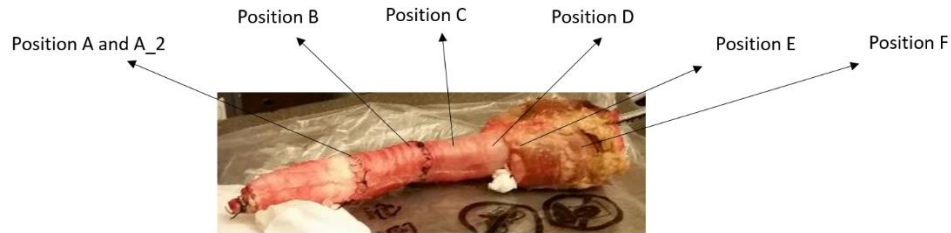


Fig 5. Porcine trachea and scan position indication

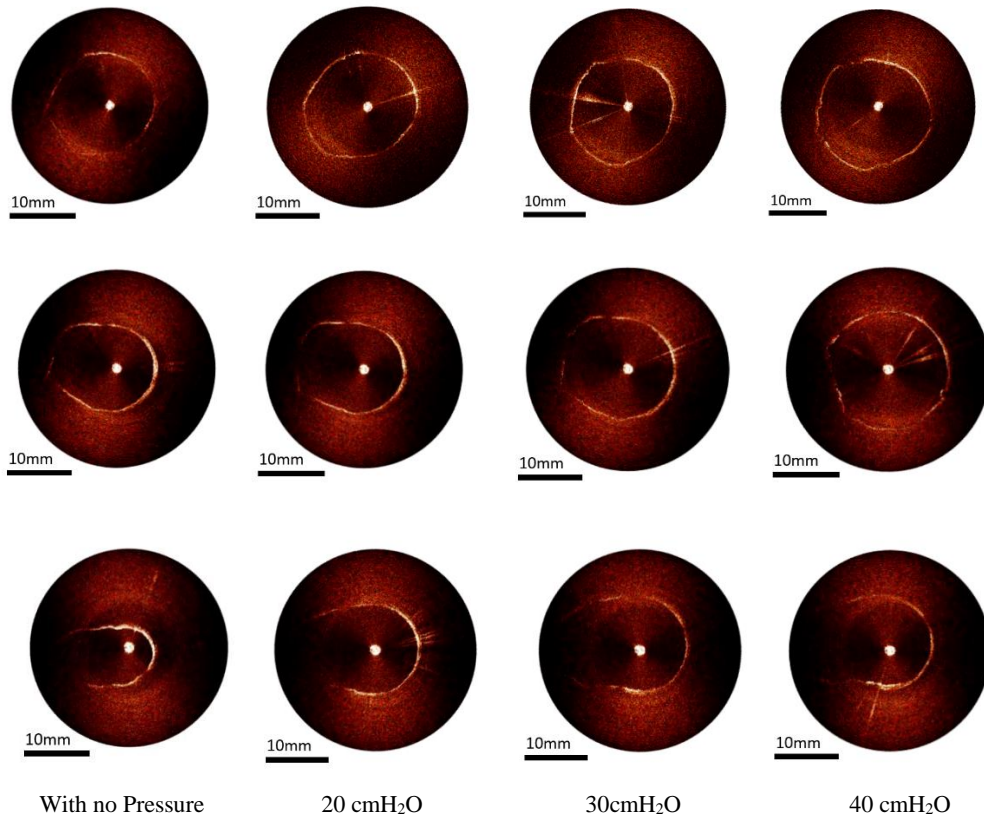


Figure 6. (a) Porcine trachea images from aOCT scan at three different positions (position A, B, C) with different pressure supply (from no pressure to pressure at 40 cmH<sub>2</sub>O);

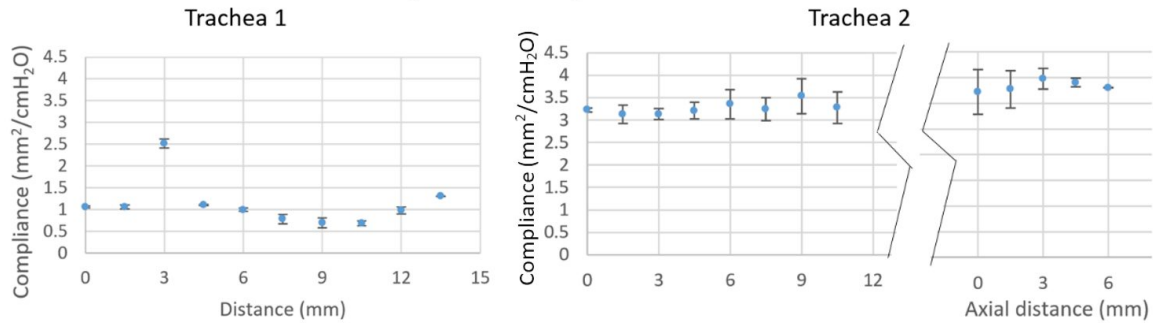


Figure 7. (a) aOCT-measured compliance at different positions across the length of each porcine trachea.

Table 2. Compliance results from porcine trachea *ex vivo* experiment

| Position   | Trachea1. A | Trachea2.A | Trachea2.B |
|--|-------------|------------|------------|
| Compliance (mm <sup>2</sup> /cmH <sub>2</sub> O) | 1.06±0.12   | 3.21±0.27  | 3.34±0.44  |
| R <sup>2</sup>                                   | 0.84        | 0.92       | 0.81       |

## 5. SUMMARY AND CONCLUSION

In this paper, we present an anatomic OCT system delivered via a conventional bronchoscope to perform elastography of the upper airway. Anatomical imaging of the tube phantom from aOCT verifies the ability to detect both circumferential and longitudinal features, while the comparison with conventional, clinical CT of the same tube highlights the higher resolution provided by aOCT. The *ex vivo* trachea CSA images from aOCT scan show characteristic structures consistent with those obtained from CT at the same positions. This suggests the potential for aOCT to be a comparable tool to that of CT for quantifying upper airway CSA.

Using aOCT for cross-sectional compliance measurements, we found the compliance of a rubber tube phantom of 0.68 mm<sup>2</sup>/cmH<sub>2</sub>O, which is consistent with the established value of 0.78 mm<sup>2</sup>/cmH<sub>2</sub>O. Furthermore, the pressure-dependent CSA data exhibits high linearity of ( $R^2 > 0.98$ ), consistent with our elasticity model. The *ex vivo* porcine experiment resulted in compliance measurements ranging from 1.06 to 3.34 mm<sup>2</sup>/cmH<sub>2</sub>O with  $R^2 > 0.81$ , indicating that the tracheas are consistent with a linearly elastic model, and that heterogeneity in the tracheas may cause changing compliance with position. At the moment, we still need further data to investigate the heterogeneity, or the structure sensitive elastography of the trachea. Improved methods to discretely localize compliance differences within individual slices are also under investigation, which may aid in building a more detailed elastography map of the trachea.

We expect that these methods could be used in future work to detect abnormal weakening of airway walls indicative of pathological states in UAOD. A primary strength of aOCT-based elastography is that it can lead to quantitative, individualized methods for treating airway disorders. The high resolution afforded by aOCT could be used for predictive modeling utilizing computational fluid dynamics simulations, which may further aid in predictive modeling and surgical decision-making.

## 6. ACKNOWLEDGEMENTS

We thank Prof. Julia Kimbell at UNC for helping us with the CT reconstruction. Dr. Nicusor Iftimia from Physical Sciences Inc. was credited with the building of the catheter and scanner. This work was funded by the National Institutes of Health, National Heart, Blood, and Lung Institute via grant R01 HL 123557 and R21 HL 111968 (Oldenburg, PI).

## REFERENCES

- [1] Myer, C. M., O'Connor, D. M. & Cotton, R. T. Proposed grading system for subglottic stenosis based on

- endotracheal tube sizes. *Ann. Otol. Rhinol. Laryngol.* **103**, 319–323 (1994).
- [2] Sher, A. E. Mechanisms of airway obstruction in Robin sequence: Implications for treatment. *Cleft Palate-Craniofacial Journal* **29**, 224–231 (1992).
- [3] Guillemineault, C., Eldridge, F. L., Tilkian, a, Simmons, F. B. & Dement, W. C. Sleep apnea syndrome due to upper airway obstruction: a review of 25 cases. *Arch. Intern. Med.* **137**, 296–300 (1977).
- [4] Pflieger, A. & Eber, E. Management of acute severe upper airway obstruction in children. *Paediatric Respiratory Reviews* **14**, 70–77 (2013).
- [5] Lowe, A. A., Fleetham, J. A., Adachi, S. & Ryan, C. F. Cephalometric and computed tomographic predictors of obstructive sleep apnea severity. *Am. J. Orthod. Dentofac. Orthop.* **107**, 589–595 (1995).
- [6] Arens, R. *et al.* Upper airway size analysis by magnetic resonance imaging of children with obstructive sleep apnea syndrome. *Am. J. Respir. Crit. Care Med.* **167**, 65–70 (2003).
- [7] Huang, D. *et al.* Optical Coherence Tomography. *Science (80-. )*. **254**, 1178–1181 (1991).
- [8] Bouma, B. *et al.* High-resolution optical coherence tomographic imaging using a mode-locked Ti:Al(2)O(3) laser source. *Opt. Lett.* **20**, 1486–1488 (1995).
- [9] Walsh, J. H. *et al.* Evaluation of pharyngeal shape and size using anatomical optical coherence tomography in individuals with and without obstructive sleep apnoea. *Journal of Sleep Research* **17**, 230–238 (2008).
- [10] Barfuss, H. & Brinkmeyer, E. Modified Optical Frequency Domain Reflectometry with High Spatial Resolution for Components of Integrated Optic Systems. *J. Light. Technol.* **7**, 3–10 (1989).
- [11] Wong, B. J. F. *et al.* In vivo optical coherence tomography of the human larynx: normative and benign pathology in 82 patients. *Laryngoscope* **115**, 1904–11 (2005).
- [12] Pitris, C. *et al.* High resolution imaging of the upper respiratory tract with optical coherence tomography: A feasibility study. *Am. J. Respir. Crit. Care Med.* **157**, 1640–1644 (1998).
- [13] Wijesundara, K. *et al.* Quantitative upper airway endoscopy with swept-source anatomical optical coherence tomography. *Biomed. Opt. Express* **5**, 788 (2014).
- [14] McLaughlin, R. A. *et al.* Applying anatomical optical coherence tomography to quantitative 3D imaging of the lower airway. *Opt. Express* **16**, 17521–17529 (2008).
- [15] Hariri, L. P., Mino-Kenudson, M., Mark, E. J. & Suter, M. J. In vivo optical coherence tomography: the role of the pathologist. *Arch. Pathol. Lab. Med.* **136**, 1492–501 (2012).
- [16] Tsuboi, M. *et al.* Optical coherence tomography in the diagnosis of bronchial lesions. *Lung Cancer* **49**, 387–394 (2005).
- [17] Williamson, J. P. *et al.* Measuring airway dimensions during bronchoscopy using anatomical optical coherence tomography. *Eur. Respir. J.* **35**, 34–41 (2010).
- [18] Armstrong, J. J. *et al.* Quantitative upper airway imaging with anatomic optical coherence tomography. *Am. J. Respir. Crit. Care Med.* **173**, 226–233 (2006).
- [19] Williamson, J. P. *et al.* Elastic properties of the central airways in obstructive lung diseases measured using anatomical optical coherence tomography. *Am. J. Respir. Crit. Care Med.* **183**, 612–619 (2011).
- [20] Krieger, A. Effect of the velopharynx on intraluminal pressures in reconstructed pharynges derived from individuals with and without sleep apnea. **367**, 173–176 (1995).
- [21] Stocks, J. Respiratory physiology during early life. *Monaldi Arch. chest Dis. = Arch. Monaldi per le Mal. del torace / Fond. Clin. del Lav. IRCCS [and] Ist. di Clin. Tisiol. e Mal. Appar. Respir. Univ. di Napoli, Second. ateneo* **54**, 358–364 (1999).
- [22] Mooney, M. A theory of large elastic deformation. *J. Appl. Phys.* **11**, 582–592 (1940).
- [23] Tozzi, P., Corno, A. & Hayoz, D. Definition of arterial compliance. *Am J Physiol Hear. Circ Physiol* **278**, H1407– (2000).
- [24] Kennedy, B. F., Kennedy, K. M. & Sampson, D. D. A review of optical coherence elastography: Fundamentals, techniques and prospects. *IEEE Journal on Selected Topics in Quantum Electronics* **20**, (2014).
- [25] Marks, D. L., Oldenburg, A. L., Reynolds, J. J. & Boppart, S. A. Autofocus Algorithm for Dispersion Correction in Optical Coherence Tomography. *Appl. Opt.* **42**, 3038 (2003).
- [26] Rogowska, J., Patel, N. a, Fujimoto, J. G. & Brezinski, M. E. Optical coherence tomographic elastography technique for measuring deformation and strain of atherosclerotic tissues. *Heart* **90**, 556–562 (2004).
- [27] Alipour, F. & Vigmostad, S. Measurement of vocal folds elastic properties for continuum modeling. *J. Voice* **26**, (2012).
- [28] Lee, K. W. & Xu, X. Y. Modelling of flow and wall behaviour in a mildly stenosed tube. *Med. Eng. Phys.* **24**, 575–586 (2002).